



Article

Influence of Screw Design and Process Parameters on the Product Quality of PEO:LiTFSI Solid Electrolytes Using Solvent-Free Melt Extrusion

Katharina Platen ^{1,*}, **Frederike Langer** ¹ and **Julian Schwenzel** ²¹ Fraunhofer Institute for Manufacturing Technology and Advanced Materials (IFAM), Lilienthalplatz 1, 38108 Braunschweig, Germany² Fraunhofer Institute for Manufacturing Technology and Advanced Materials (IFAM), Wiener Straße 12, 28359 Bremen, Germany

* Correspondence: katharina.platen@ifam.fraunhofer.de

Abstract: All-solid-state battery (ASSB) technology is a new energy system that reduces the safety concerns and improves the battery performance of conventional lithium-ion batteries (LIB). The increasing demand for such new energy systems makes the transition from laboratory scale production of ASSB components to larger scale essential. Therefore, this study investigates the dry extrusion of poly(ethylene oxide):lithium bis (trifluoromethylsulfonyl)imide (PEO:LiTFSI) all-solid-state electrolytes at a ratio of 20:1 (EO:Li). We investigated the influence of different extruder setups on the product quality. For this purpose, different screw designs consisting of conveying, kneading and mixing elements are evaluated. To do so, a completely dry and solvent-free production of PEO:LiTFSI electrolytes using a co-rotating, intermeshing, twin-screw extruder under an inert condition was successfully carried out. The experiments showed that the screw design consisting of kneading elements gives the best results in terms of process stability and homogeneous mixing of the electrolyte components. Electrochemical impedance spectroscopy was used to determine the lithium-ion conductivity. All electrolytes produced had an ionic conductivity (σ_{ionic}) of $(1.1\text{--}1.8) \times 10^{-4} \text{ S cm}^{-1}$ at 80°C .



Citation: Platen, K.; Langer, F.; Schwenzel, J. Influence of Screw Design and Process Parameters on the Product Quality of PEO:LiTFSI Solid Electrolytes Using Solvent-Free Melt Extrusion. *Batteries* **2024**, *10*, 183. <https://doi.org/10.3390/batteries10060183>

Academic Editors: Juan Carlos Gonzalez-Rosillo and Moran Balaish

Received: 30 April 2024

Revised: 17 May 2024

Accepted: 22 May 2024

Published: 28 May 2024



Copyright: © 2024 by the authors. Licensee MDPI, Basel, Switzerland. This article is an open access article distributed under the terms and conditions of the Creative Commons Attribution (CC BY) license (<https://creativecommons.org/licenses/by/4.0/>).

1. Introduction

Lithium-ion batteries (LIBs) have become an indispensable part of modern life. However, there are still safety [1,2] and toxicity [3–6] issues with the use of commercial LIBs with organic liquid electrolytes. To solve this problem, the organic liquid electrolyte can be replaced with ion-conducting, non-volatile and less flammable solid materials for use in all-solid-state batteries (ASSB) [7]. Materials that are used as solid electrolytes are generally divided into three material classes: polymers, oxides and sulfides [8–10]. The use of ion-conducting solids as electrolytes, which have a certain mechanical stability to suppress lithium dendrite formation [7,11,12], allows the use of lithium metal as anode material. This results in higher capacity and cell voltage than conventional LIBs. The safety of an ASSB can be improved by using a non-volatile and less flammable material as the electrolyte such as polymers [13]. Further, due to their malleable and elastic nature, they are able to compensate for large volume changes in the electrodes during discharging and charging processes [14]. Recent approaches for polymer electrolytes have been made to improve the ionic conductivity [15,16] and the mechanical strength against Li metal [17,18].

The high demand and interest in ASSBs require the transition of production of ASSB components from laboratory scale to larger scale production. Electrolyte materials for ASSBs have been extensively studied in terms of their electrochemical performance and

their stability against electrode materials. However, the commercialization of these materials is still hindered due to unavailability of materials in larger quantities in the case of oxides and sulfides and the lack of knowledge on scaled up production routes [19]. The availability of polymers in the global market encourages manufacturers to focus more on the processing routes of solid polymer electrolytes (SPEs) considering their manufacturability and cost. Recently, SPEs have been produced by solvent-based methods such as solution casting [20–27], which requires several steps, i.e., premixing of the solid fraction, preparing a slurry and drying of the electrolyte to remove the solvent from the SPE. In addition, solvent residues affect both the electrochemical performance and the mechanical properties of the polymer [28]. In addition, comparing solvent-based processing routes with dry production, significant reductions in investment, operating costs and energy consumption are expected [29–31].

For this reason, a processing method such as hot pressing [20,32–34] or extrusion [35–37], which does not require solvents, is preferable for upscaling. For SPE production, extrusion is more suitable due to its continuous mode of operation and high throughput. Further, compared to hot pressing, extrusion allows for the production of SPEs in the desired shape using suitable dies and the process can be easily implemented in an automated process line. In addition, the SPE components can be processed without any preparation as powders. The extrusion also provides excellent mixing of the components, resulting in a homogenous mixture and ensures uniform distribution of the components.

Thermal production of SPEs requires the use of thermoplastics as a polymer matrix.

A widely used thermoplastic for SPEs is poly(ethylene oxide) (PEO) [38–42]. PEO has a melting temperature (T_m) ~ 65 °C depending on the molecular weight (M_w) [43]. Furthermore, PEO has the ability to dissolve alkali metal salts, such as lithium bis (tri-fluoromethylsulfonyl)imide (LiTFSI), forming a (PEO)-Li salt complex [44]. In addition, LiTFSI affects the thermal properties and crystallization behavior of PEO [38–41]. It acts as a plasticizer, which enhances the flowability of PEO during thermal processing. In the case of high M_w PEO, it even accelerates chain scission of the polymer chains, thereby reducing M_w [45]. In addition, high M_w PEO is very sensitive towards high temperatures and mechanical stress. We have recently shown that PEO with a M_w of 100,000 g mol⁻¹ is more suitable for thermal production of SPEs than PEO with M_w of 600,000 g mol⁻¹ [45]. Nevertheless, care must be taken to avoid degradation of PEO by optimizing process parameters (process temperature and screw speed) for thermal production.

This study focuses on the effects of different screw designs on the mixing behavior of PEO and LiTFSI using a co-rotating twin-screw extruder. The aim is to evaluate the influence of screw design and process parameters on PEO:LiTFSI electrolytes at a molar ratio of 20:1 (EO:Li). It is known that PEO becomes stickier with increasing salt content [40,46]. Therefore, the mixing ratio of 20:1 (EO:Li) is used due to its better handling during sample extraction after extrusion and its relatively high ionic conductivity at elevated temperatures. The screws are designed with conveying, kneading and mixing elements. The pressure at the extruder die and torque are continuously measured during the production. Process temperature and screw speed are optimized to avoid PEO degradation. Products are evaluated for homogeneity and quality of the extruded electrolytes. Optical microscopy is used for macroscopic evaluation, and rheology measurement is performed to determine loss of molecular weight. Electrochemical impedance spectroscopy (EIS) is used to assess the ionic conductivity.

2. Materials and Methods

2.1. Materials

As electrolyte materials, PEO (POLYOX WSR N10, IFF, New York, NY, USA) (nominal weight $M_w = 100,000$ g mol⁻¹) is used as thermoplastic polymer and LiTFSI (Carbolution Chemicals GmbH, St. Ingbert, Germany) as conductive salt. All components are dried under vacuum for 12 h before use. Prior to extrusion, PEO and LiTFSI powders were mixed

in a ratio of 20:1 (EO:Li) for 30 min using a TURBULA[®]-mixer (Willy A. Bachofen AG, Muttenz, Switzerland).

2.2. Extruder Setup

All extrusion experiments are carried out in an argon-filled glovebox (H_2O and $\text{O}_2 < 1 \text{ ppm}$) with a co-rotating, intermeshing, twin-screw extruder with a total screw length of 576 mm (ThreeTec, Seon, Switzerland). The twin-screw has segmental screw elements with a length of 36 mm per screw segment. Different screw elements can be placed at a desired location along the screw. The screw design was varied by changing the screw elements between heating zone 3 and 4 (see Figure 1). The screw elements used in this work were conveying elements (screw design A), kneading elements (screw design B) and mixing elements (screw design C). The screw elements are identical in the basic construction and differ only in their functionality. Each element has a pitch of 24 mm, a L/D of 24/36, a thread angle of $\sim 17.7^\circ$ and a d_o/d_i of 24/16. The main difference is that the kneading elements have a $4 \times 60^\circ$ angle block construction and the mixing elements have mixing shafts along the length of the screw element. As mentioned above, these elements are assembled in the screw design, where we expect a complete melting of the PEO, so the assumed dominant force is the viscous energy dissipation (VED). A 3 mm string nozzle was used to shape the polymer electrolyte and to improve sample extraction.

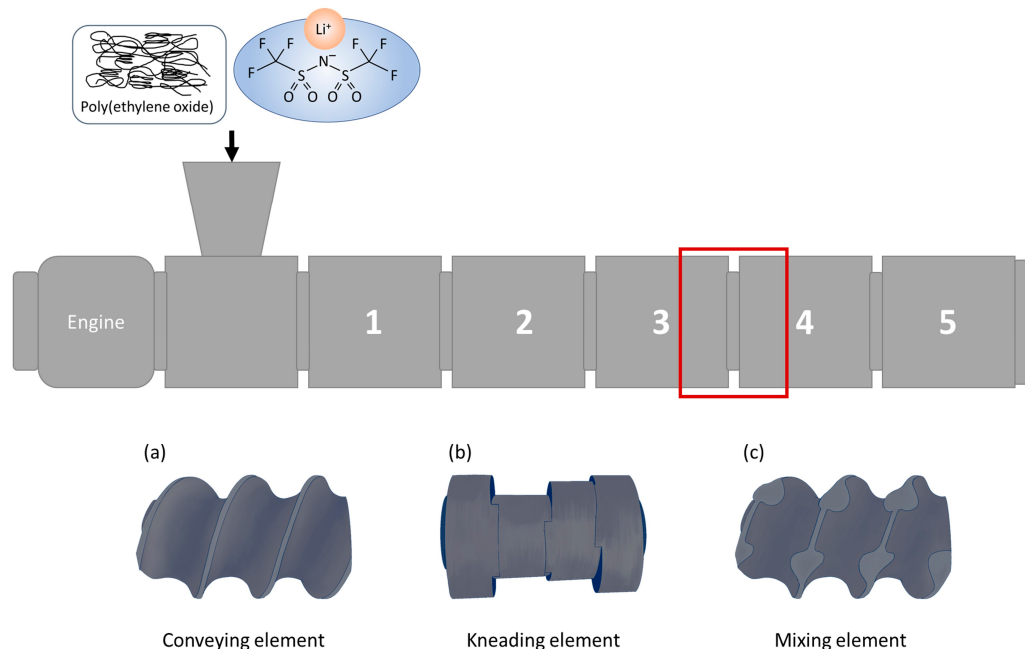


Figure 1. Scheme of the extruder setup for the extrusion of pre-mixed $\text{PEO}_{20}\text{LiTFSI}$ powder batch and the used screw elements: a: conveying element, b: kneading element and c: mixing element. The total screw length of the extruder is 576 mm. The feeder used in this work has a material capacity of 9 L. The sketches of the PEO and the LiTFSI are taken from previous work [45].

According to our previous observations [45], all experiments are carried out with a constant barrel temperature of 90°C and screw speeds of 5, 10 and 15 rpm. During the experiment, the process parameters, including the pressure at the extruder die and torque, are measured continuously. After 30 min of extrusion, the screw speeds are gradually increased. After 20 min, the process is considered to be in a steady state, and sample and process parameters are taken within the last 10 min for each screw speed.

2.3. Digital Microscopy Observations

The extruded samples were characterized macroscopically using a digital microscope VHX7000 (Keyence, Osaka, Japan) with incident light. To handle the samples outside the

glovebox, the extruded $\text{PEO}_{20}\text{LiTFSI}$ strings were hermetically sealed in Petri dishes. To correctly determine the color of the sample, a white balance was performed before the image was taken.

2.4. Rheology Measurements

Rheology measurements are performed to determine the M_w of each polymer electrolyte produced after extrusion. Therefore, the viscosity of 5 wt%-aq. polymer solutions is determined at 25 °C using a rotational rheometer (MCR702, Anton Paar, Graz, Austria) using a cone-plate geometry (50 mm/1°) at a constant shear rate of 50 s⁻¹ for 10 min.

2.5. Dynamic Mechanical Analysis

To determine the thermo-mechanical properties of the produced polymer electrolytes, temperature-dependent dynamic mechanical analysis (DMA) is used. The polymer electrolytes were hot pressed at 90 °C to a thickness of 1 mm and were then punched to a diameter of 25 mm. DMA measurements were performed using an oscillating rheometer (MCR702, Anton Paar, Graz, Austria) using a 25 mm plate geometry at 1 Hz and a deformation amplitude of 0.1% in a temperature range of 20–100 °C with a heating ramp of 1 K min⁻¹. The results obtained are the temperature-dependent storage modulus G' and loss modulus G'' , where G' and G'' represent the elastic and the viscous portions of $|G^*|$, respectively.

2.6. Electrochemical Impedance Spectroscopy

Electrochemical impedance spectroscopy measurements were performed with an Interface 1010E (GAMRY Instruments Inc., Warminster, PA, USA). The extruded PEO electrolytes were prepared by hot pressing to a thickness of 280 µm and contact with aluminum blocking electrodes. The symmetrical cells were tested in KP solid cells (Hohsen), and the frequencies were varied from 10⁶ Hz to 1 Hz with an amplitude of 10 mV. The impedance data were fitted with an equivalent circuit consisting of a parallel R-CPE element, where the resistance is attributed to the ionic resistance of the polymer electrolyte. The ionic conductivity σ_{ionic} at 80 °C can be calculated from the sample geometry.

2.7. Electrochemical Cycling Experiments

Electrochemical cycling experiments were performed with a BaSyTest (BaSyTec GmbH, Asselfingen, Germany). The extruded PEO electrolytes were prepared by hot pressing to a thickness of 280 µm and assembled in a 2032-coin cell using Li metal as the anode (MSE Supplies®, Tuscon, AZ, USA, 14 mm) and an LFP cathode (12 mm). The LFP cathode consisted of LFP active material (Life Power P2, Clariant, Muttenz, Switzerland), PVdF as binder (Solef 5130 PVdF, SOLVAY, Brussel, Belgium) and Super C65 (Imerys Graphite & Carbon, Willebroek, Belgium) as electronically conductive additive in a ratio of 90 wt%, 4 wt% and 6 wt%, respectively. Cell assembling was carried out in a glovebox (H_2O and O_2 < 0.1 ppm). For each electrolyte, three coin cells were prepared for testing. Prior to cycling, the coin cells went through a formation step using a constant current of 0.05 C for three cycles. Constant current constant voltage (CCCV) cycling at 0.1 C was performed for 20 cycles at 80 °C between 2.8 V and 3.6 V.

3. Results and Discussion

3.1. Extrusion of $\text{PEO}_{20}\text{LiTFSI}$ Electrolytes

The process parameters are continuously monitored after the extruder is started and the barrel is filled. To define a steady state condition for each extruder setup, the torque and pressure values are extracted from the last 10 min of extrusion as described above. Process stability can be interpreted as a measure of the size of the error bars. The screw elements differ only in functionality, and they are assembled in the VED region. The shear force that causes this dissipation comes from the screw elements. Therefore, the effects on the process and product quality described below can be traced back to the screw elements.

The left diagram in Figure 2 shows the measured torque for the three screw designs (A, B and C) as a function of the applied screw speeds. It is clearly visible that the torque increases with the applied screw speed for all three screw designs. The smallest error bars and, thus, the most stable process can be observed for all three screw designs at a low screw speed of 5 rpm. Here, screw design A shows the largest (± 0.82 Nm) and screw design C shows the smallest (± 0.09 Nm) error bar. At low screw speeds, the residence time of the material in the extruder barrel is longer. The longer the residence time of PEO in the extruder barrel, the more time PEO has to melt and to dissolve LiTFSI. This applies for any screw design. Due to the plasticizing effect of LiTFSI [47] and by enhancing the flowability of PEO, less energy is required to transfer the material through the barrel. However, screw design B shows a smaller error bar at 15 rpm than at 10 rpm. Here, the screw speed and the higher energy input of the kneading elements compared to the other screw designs reduce inhomogeneities in the melt and improve the mixing and dissolving of LiTFSI. This allows the engine of the extruder to maintain the energy required to keep the screw speed more stable.

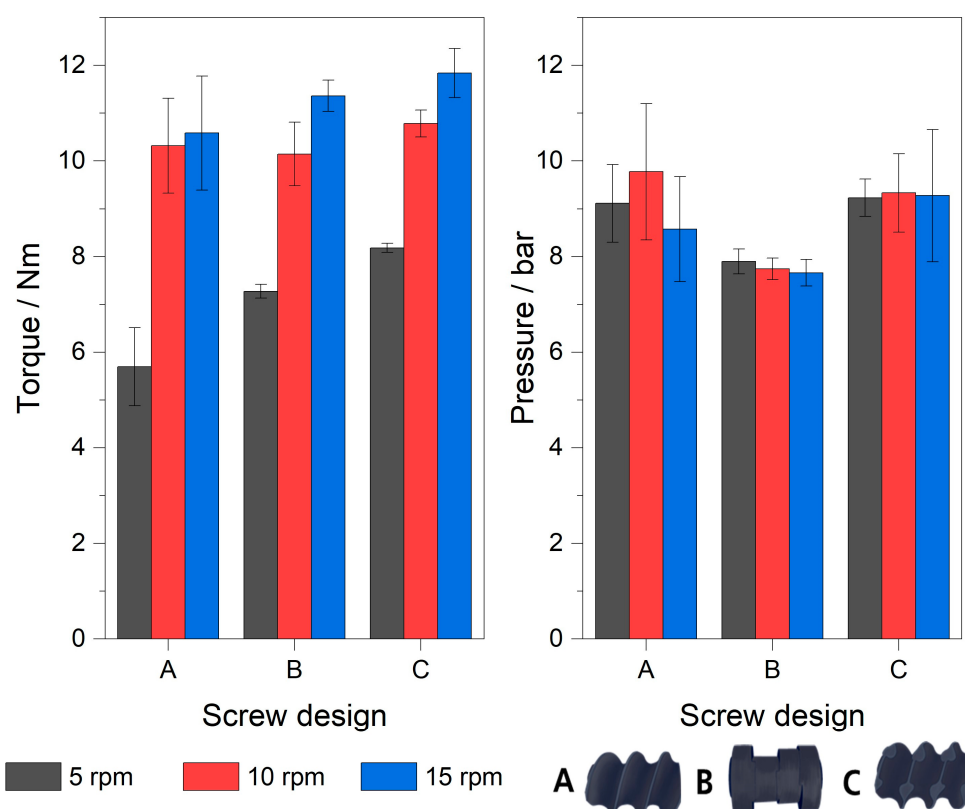


Figure 2. Measured torque (left) and pressure at the extruder die (right) during extrusion extracted from the last 10 min of the process dependent of the applied screw speed for each screw design.

The measured pressure at the extruder die for all three screw designs as a function of the applied screw speed is visualized in the right diagram in Figure 2. The pressure does not show any significant change with the applied screw speed. Screw design B shows the lowest pressure with 7.7–7.9 bar as well as the smallest error bar ($<\pm 3$ Nm) for all three screw speeds. The low pressure can be explained by the longer residence time of the material in the extruder barrel due to the kneading elements in the screw design and the associated plasticizing by mixing with LiTFSI. Kneading elements hold the material in front of each kneading block until there is sufficient material accumulation to push the material forward and overcome the retention force of the kneading block. In addition, dispersive mixing dominates around the kneading elements. Due to the higher shear effects, more energy is transferred into the polymer, resulting in a higher flowability of the material [48].

As mentioned earlier, the residence time plays an important role for the mixing. Here, we define the residence time of the component by the material output. Therefore, we assume that the higher the output per hour, the shorter the residence time. Figure 3 shows the correlation between the measured process parameters and the material output. The diagram clearly shows that the output is greatly reduced from 1.6 kg h^{-1} to $<1.0 \text{ kg h}^{-1}$ using screw designs B and C. Torque increases with higher output because the extruder engine must exert more energy to transport more material through the extruder. The pressure is more influenced by the screw configurations themselves, resulting in the lowest pressure for screw configuration B. As already assumed earlier, screw configuration B has the longest residence time of the components characterized by the lowest overall output.

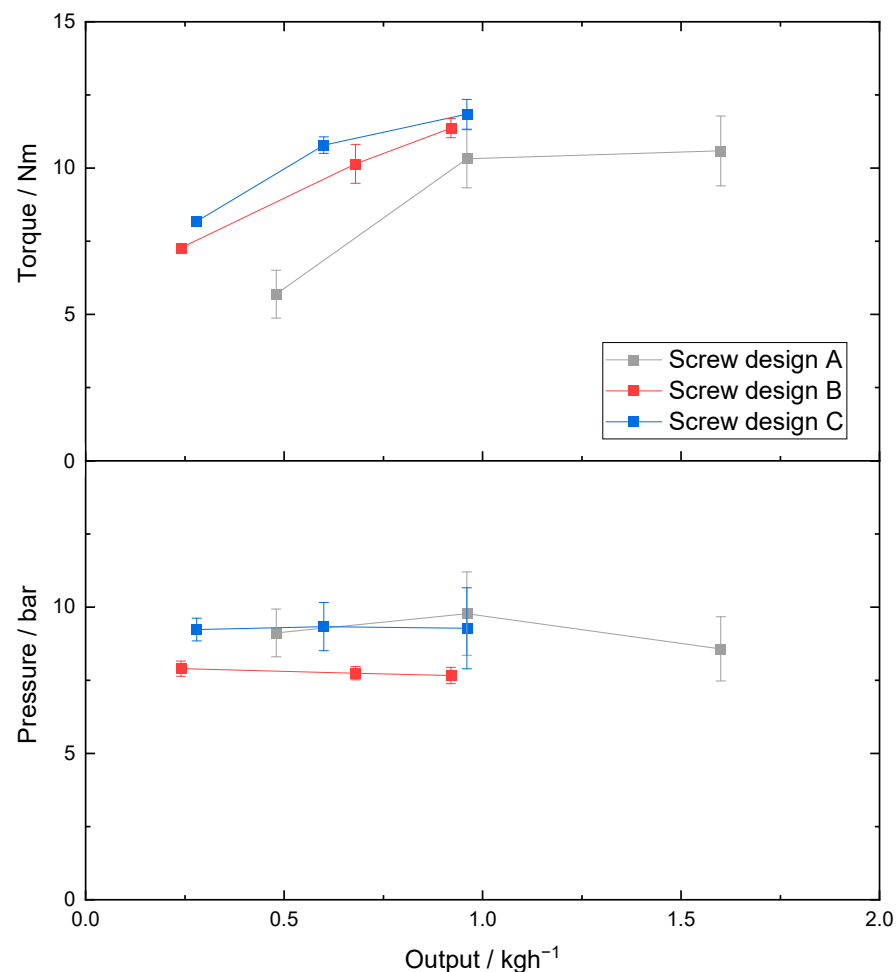


Figure 3. Correlation between extruder parameters measured during extrusion and material output; lines are guide for eyes.

3.2. Microscopic Observation

For product characterization, microscopic observations are made to determine the mixing and dissolution of LiTFSI into the polymer matrix during extrusion. Figure 4 shows microscopic images of extruded electrolytes as a function of the used screw design and the applied screw speed. For a better color representation, the RGB model of each sample is shown as a bar over the microscopic image. The samples show a color gradient indicating different mixing states depending on the screw design and applied screw speed. White PEO powder turns yellow after thermal treatment. The darker the color, the more PEO is affected by degradation [45]. The addition of LiTFSI causes the PEO to become whiter and lighter in color. Therefore, the samples with a more yellowish hue are classified as poorly mixed and the samples with a whiter hue as well mixed. All produced electrolytes show a smooth

and shiny surface for all screw designs. This indicates that the polymeric material does not go through a degradation process during extrusion that damages the outer appearance of the material. All screw designs show different mixing results. The irregular shape of the extruded sample is a result of uneven pull-off during sample extraction. Since this does not affect the mixing during extrusion and the samples are post processed by hot pressing before electrochemical characterization, the shape of the sample is neglected in this work. Screw design A (Figure 4a,c) shows good mixing of the components at screw speeds of 5 and 15 rpm. The higher pressure at the extruder die at the screw speed of 10 rpm (s. Figure 2) compared to the other screw speeds indicates that LiTFSI is not well dissolved in the PEO matrix. This is also indicated by the more yellowish color of the extruded electrolyte (Figure 4b). While the mixing and dissolving of LiTFSI in the PEO matrix improves with a higher screw speed for screw design B (Figure 4d–f), the extruded electrolytes with screw design C (Figure 4g–i) show an opposite mixing and dissolving behavior.

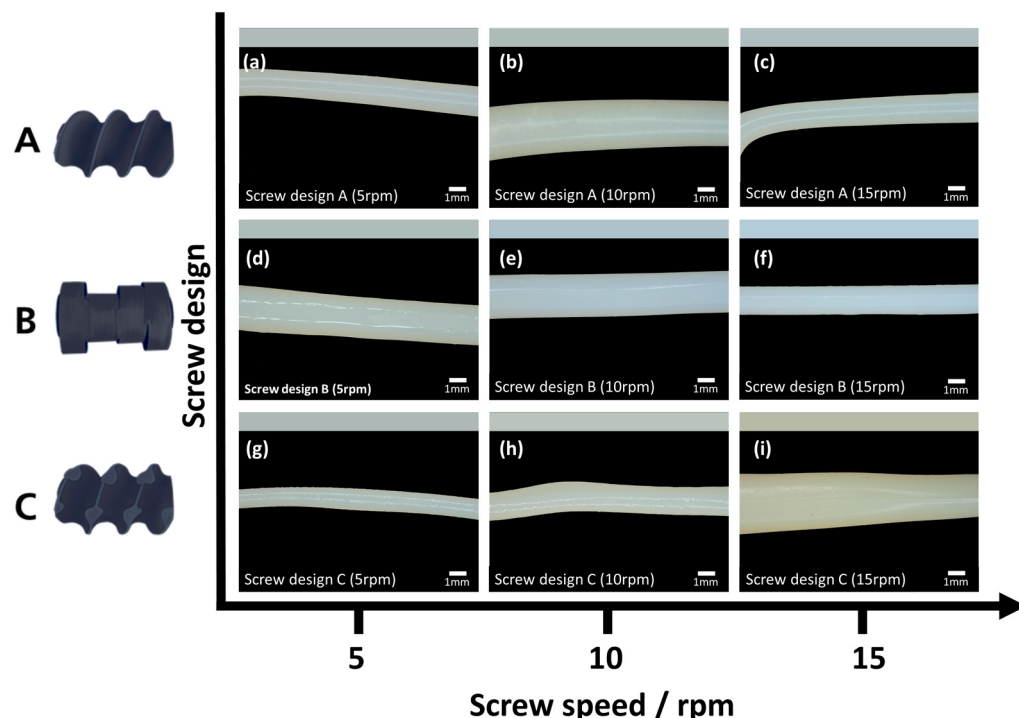


Figure 4. Digital microscopy images of extruded PEO20LiTFSI electrolytes with different screw designs and applied screw speeds (a–c): screw design A at 5–15 rpm, (d–f): screw design B at 5–15 rpm and (g–i): screw design C at 5–15 rpm. The RGB model of each sample is shown as a bar over the microscopic image for a better color representation. Samples with a more yellowish hue are classified as poorly mixed and the samples with a whiter hue as well mixed.

The best mixing is shown for screw design B with an applied screw speed of 15 rpm (Figure 4f). Here, the kneading elements and the high shear stress improve the mixing and dissolution of LiTFSI in the PEO matrix, which is also characterized by the lowest pressure in Figure 2. In comparison, screw design C (Figure 4i), with an applied screw speed of 15 rpm, shows the yellowest sample indicating poor mixing. Despite the use of mixing elements, this screw design does not seem to be suitable for the extrusion of PEO:LiTFSI electrolytes, especially at high screw speeds.

3.3. Determination of Molecular Weight

The molecular weight of the extruded polymer electrolytes is examined to determine whether the properties of the polymer are maintained or whether degradation in the form of chain scission occurs during extrusion. The molecular weight (M_w) of each PEO:LiTFSI electrolyte after extrusion is determined from the viscosity of 5 wt%-aq. polymer solu-

tions at 25 °C. We found that the viscosity correlates with the determined M_w via GPC measurements from earlier work [45], and using this correlation it is possible to calculate the M_w from the viscosities of the electrolytes. Figure 5 shows a reduction in M_w after extrusion for all three screw designs and applied screw speeds. The extruded PEO:LiTFSI electrolytes with screw design A show the largest reduction with 42% (5 rpm). There is no real trend as a function of the screw speed. While screw design A shows no dependence on the screw speed, the M_w of PEO:LiTFSI electrolytes decreases for screw design B at lower screw speeds and for screw design C at higher screw speeds.

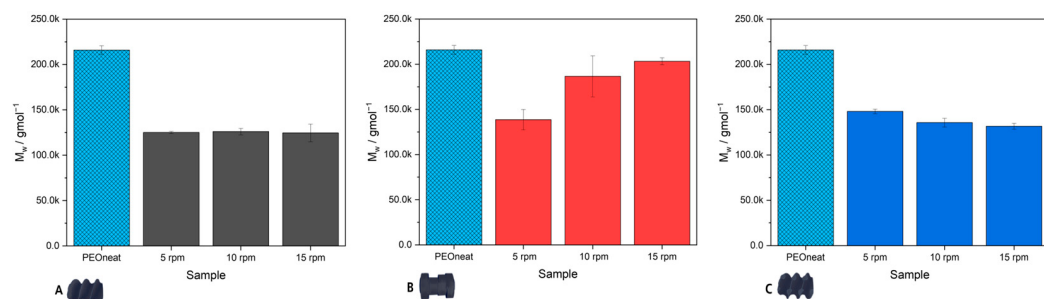


Figure 5. Molecular weight of extruded PEO:LiTFSI electrolytes dependent on the screw design and the applied screw speed compared to the molecular weight of pristine PEO. The light blue bar with a pattern is the determined M_w for pristine PEO and is used for all three diagrams as a reference. The bars representing the determined M_w of the PEO:LiTFSI-electrolytes are colored in gray, red, and blue for a better assignment to the screw designs A, B, and C, respectively.

Although Figure 2 shows a dependence of the measured torque and pressure on the applied screw speed, no correlation can be defined between the measured process parameter and the determined M_w for screw design A. This is different for the other two screw designs B and C. For screw design B, the measured process parameters indicate that more energy is transferred into the material with increasing screw speed, characterized by higher torque values and decreasing pressure at the die, but the determined M_w shows contradictory behavior. One would expect a similar dependence of M_w on the process parameters as seen for screw design C. Since the pressure at the extruder die does not depend on the screw speed, the dominant force is the torque of the screws themselves. As shown in Figure 2, the torque increases with increasing screw speed, resulting in a decrease in M_w , indicating chain scission during extrusion.

For a screw speed of 15 rpm, the M_w of the electrolytes shows that screw design B has the smallest reduction. This indicates that this extruder setup is the most suitable to maintain the polymer properties and at the same time, as shown in Figure 4, gives the best result in mixing the components while having the highest throughput.

3.4. Dynamic Mechanical Analysis

Figure 6 shows the determined temperature-dependent mechanical properties using DMA. The storage modulus (G') and the loss modulus (G'') are depicted for neat PEO and the extruded PEO:LiTFSI electrolytes using different screw designs and a screw speed of 15 rpm. G' and G'' represent the elastic and viscous portion of the material, respectively. The melting temperature (T_m) of each sample is determined by the onset of the drop in the G' curve. The curves of all investigated samples can be divided into two sections. The first section ($T < T_m$) is dominated by the elastic portion ($G' > G''$) of the materials. The samples are in solid-state. In the second section ($T > T_m$), the viscous portion ($G' < G''$) dominates. The samples are in liquid-state/molten-state. The melting of PEO is characterized by the large drop in both curves and in the huge loss of mechanical strength. The polymer electrolytes show a melting temperature 10 °C lower than PEO without conducting salt. This is due to the incorporation of the conducting salt. In addition, all polymer electrolytes produced exhibit lower stiffness than pure PEO over the whole temperature range. This is

also attributed to the conductive salt, which acts as a plasticizer and reduces the mechanical properties of the PEO. The stiffness in the melt is slightly different for all four samples. However, the PEO:LiTFSI electrolyte produced with screw design C has higher G' and G'' values compared to the electrolytes produced with screw designs A and B. This indicates that less LiTFSI is mixed into the polymer, making it less soft than the other electrolytes and reinforces the findings of the microscopic characterization (Figure 4i).

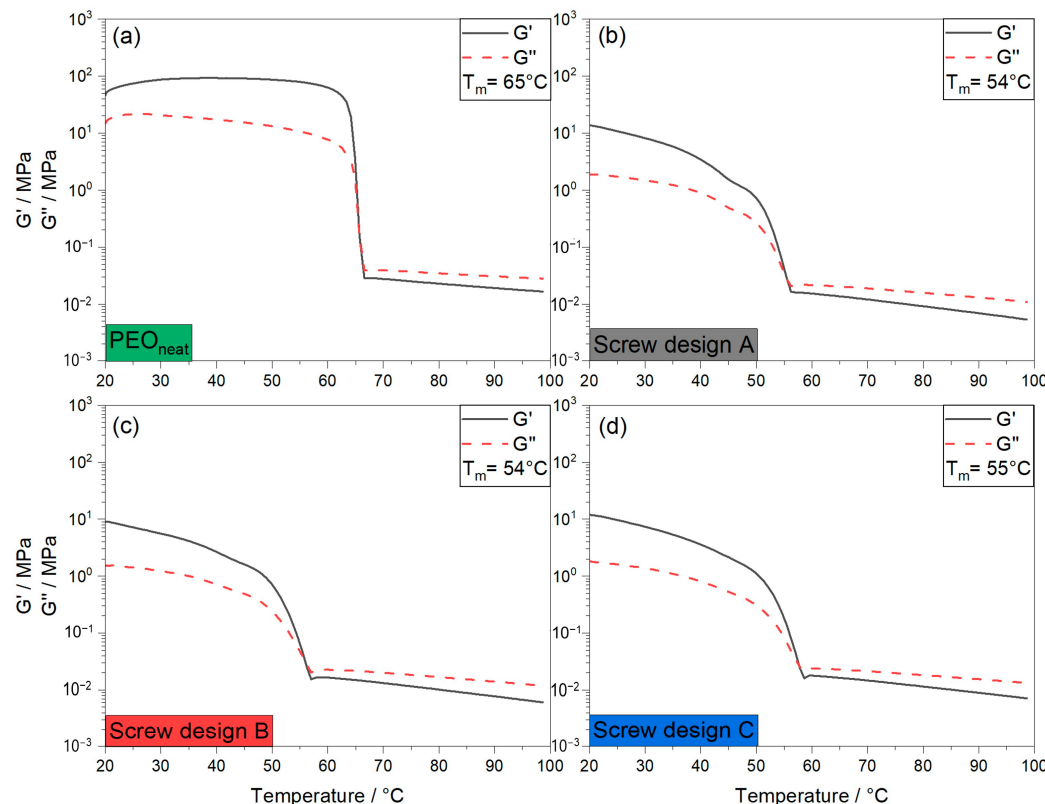


Figure 6. Temperature-dependent storage modulus G' (solid line) and loss modulus G'' (dotted line) for neat PEO and extruded PEO:LiTFSI electrolytes with different screw designs at a screw speed of 15 rpm. (a) neat PEO; (b) PEO:LiTFSI electrolyte extruded with screw design A; (c) PEO:LiTFSI electrolyte extruded with screw design B; (d) PEO:LiTFSI electrolyte extruded with screw design C.

3.5. Electrochemical Characterization

Electrochemical impedance spectroscopy at $80\text{ }^\circ\text{C}$ is used to determine the Li-ionic conductivity (σ_{ionic}) of the polymer electrolytes.

As shown in Figure 7, all impedance data are fitted with an equivalent circuit consisting of an R_{SPE} and a CPE element. The resistance R_{SPE} is usually attributed to the ionic resistance originating from the polymer electrolyte and the CPE element to the blocking electrodes. The conductivity can be calculated from the determined R considering the sample geometry. Figure 8 shows the σ_{ionic} for PEO-based electrolytes as a function of their molar ratio (EO:Li) and their preparation extracted from the literature [13,33,49–54]. The diagram clearly shows that solvent-based electrolyte preparation is still widely used in research as solvent-free preparation methods covering a wide range of mixing ratios. The solvent-based prepared electrolytes presented are generally prepared by solvent casting of dissolved PEO and LiTFSI in acetonitrile [49,54–56]. The solvent-free preparations are performed by mechanical mixing or hot pressing at $100\text{--}120\text{ }^\circ\text{C}$ [33,51,52] or simple pressing [53] of the components. Nevertheless, the presented σ_{ionic} shows no clear trend depending on the sample preparation. Thus, it is even possible to compare the σ_{ionic} of electrolytes produced in this work with the σ_{ionic} electrolyte prepared by the solvent-based method. Overall, all produced PEO:LiTFSI electrolytes show an σ_{ionic} between

$1.1 \times 10^{-4} \text{ S cm}^{-1}$ and $1.8 \times 10^{-4} \text{ S cm}^{-1}$ at 80°C , which is comparable to the literature indicating successful production of PEO-based electrolytes. Furthermore, although all the produced PEO-based electrolytes show a decrease in M_w after extrusion, the M_w seems to be high enough to not affect the σ_{ionic} of the electrolytes. This is in good agreement with the findings of Hallinan et al. where the authors present an exponential relationship between σ_{ionic} and M_w , when $M_w < 2000 \text{ gmol}^{-1}$ [57]. PEO-based electrolytes with $M_w > 2000 \text{ gmol}^{-1}$ have no influence on the σ_{ionic} .

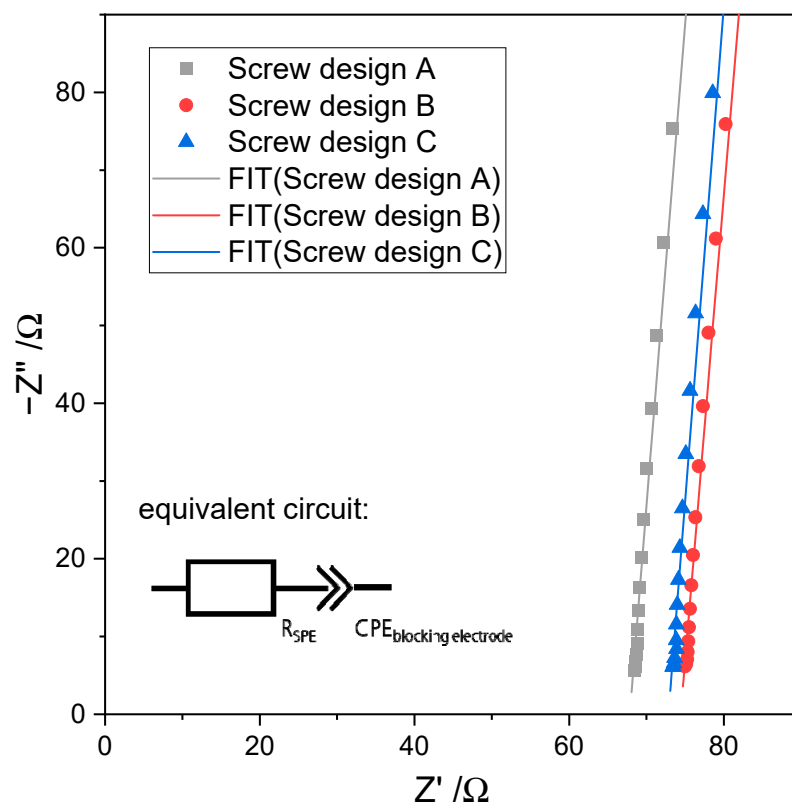


Figure 7. Exemplary Nyquist plot of impedance measurement of PEO:LiTFSI electrolytes at 80°C extruded with different screw designs and an applied screw speed of 15 rpm; measured thickness of electrolytes screw design A: $0.292 \mu\text{m}$, screw design B: $0.362 \mu\text{m}$, screw design C: $0.275 \mu\text{m}$.

For the investigation of the electrochemical behavior of the PEO:LiTFSI electrolytes produced, cycling tests were performed in a 2032-coin cell setup. Figure 9a depicts the charge and discharge curves at 80°C for the first cycle in the potential window of 2.8 V to 3.6 V vs. Li^+/Li depending on the screw designs used. All three cells show the characteristic charge and discharge plateau of LFP at around 3.4 V. The specific capacity achieved varies with the screw design used. While the full cell with the PEO:LiTFSI electrolyte produced with screw design A reaches a specific capacity of 145 mAh g^{-1} , the cells with PEO:LiTFSI electrolyte produced with screw design C reaches the lowest specific capacity of 115 mAh g^{-1} . The theoretical capacity of 150 mAh g^{-1} of LFP was not achieved by any of the systems studied. A possible reason for this is the use of a conventional cathode structure without additional catholyte, which might prevent the complete infiltration of the cathode layer. This means that not all active material particles are reached and contribute to the achieved capacity of the cells. These results are in agreement with the thermo-mechanical properties of the PEO:LiTFSI electrolytes. The lower specific capacity for screw design C can result in a higher resistance of the PEO:LiTFSI electrolyte. This resistance is characterized by the higher G' and G'' values at 80°C compared to the electrolytes produced with the other screw designs. In addition, the lower calculated σ_{ionic} for screw design C, which allows for less Li-ion migration during the charge and discharge, can also result in a lower

specific capacity. Comparing the charge curves of the screw designs, the higher resistance of the electrolyte of screw design C may also be responsible for the shift of the characteristic plateau of LFP to higher potentials.

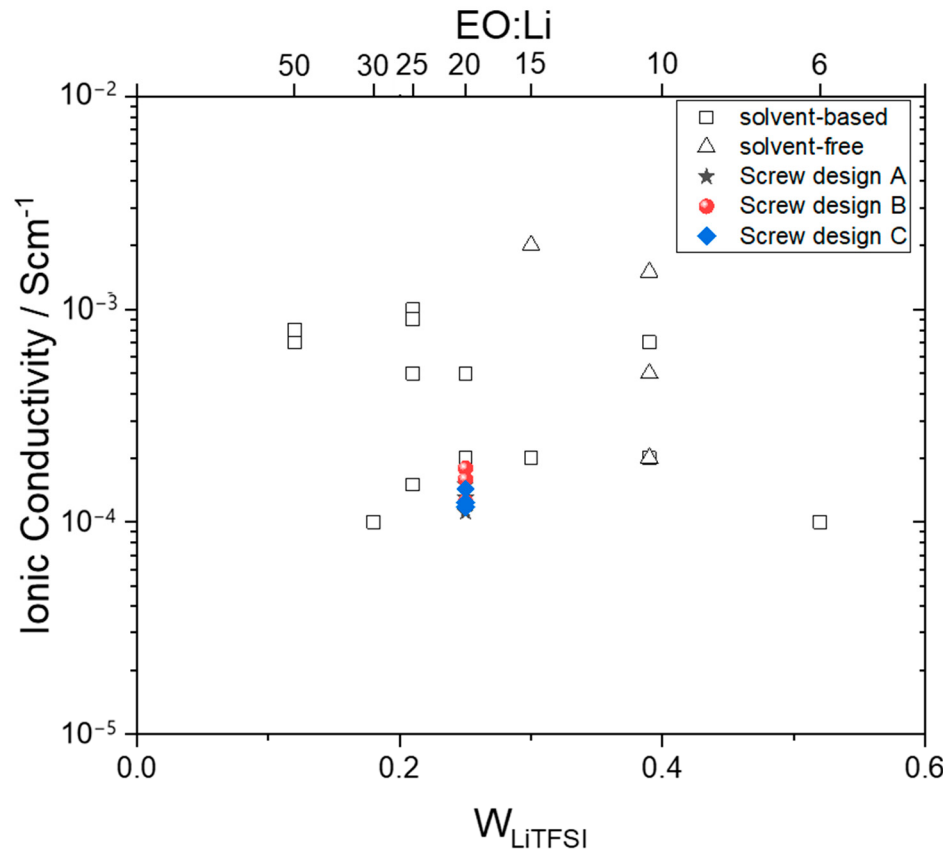


Figure 8. Ionic conductivity (σ_{ionic}) of extruded PEO:LTSI electrolytes compared to the literature values of σ_{ionic} of PEO:LTSI electrolytes produced by solvent-based (rectangles) and solvent-free methods (triangles); for comparison, it should be noted that the extracted σ_{ionic} values are based on PEO systems with different M_w ; single data of σ_{ionic} depending on the M_w according to the literature are listed in Appendix A.

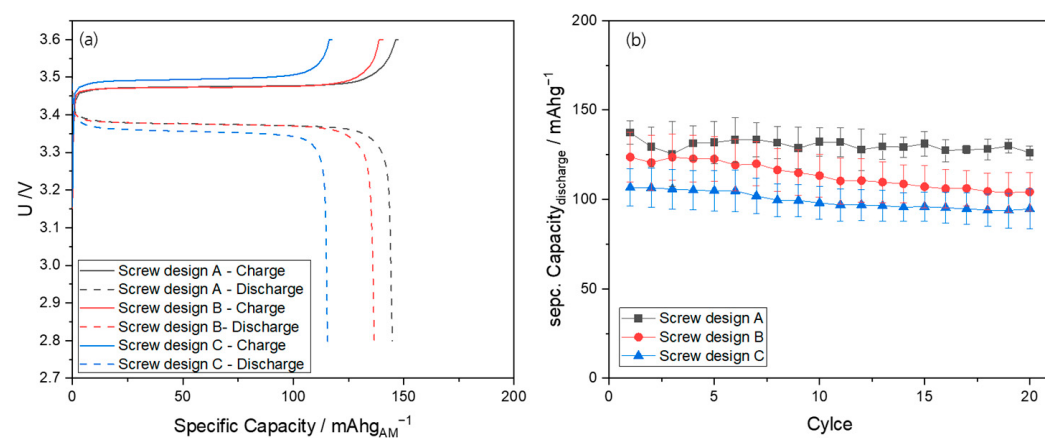


Figure 9. Electrochemical cycling experiments of extruded PEO:LTSI electrolytes. (a) Depicts the charge and discharge curves for the first cycle with the characteristic plateau of the LFP cathode; (b) shows the average of the specific capacity for discharging the cells for 20 cycles of three measured cells.

Figure 9b shows the specific capacity for discharging of the cells for 20 cycles. The electrochemical behavior as described above for Figure 9a remains constant over the 20 cycles measured. The cells of screw design A show the lowest total loss in specific capacity of 3.8%, and the cells of screw design B show the highest total loss in specific capacity of 15% over the 20 cycles. As can also be observed from Figure 9a, the cells of screw design C show the lowest specific capacity over the 20 cycles with a total loss of 11%. Although PEO:LiTFSI electrolytes prepared with screw design B appear to be the most promising from the previous investigations, the cells perform the worst in the cycling test, as indicated by the high specific capacity loss in a full cell. As shown by the microscopy, rheological investigations and EIS measurements, a possible cause may be the higher amount of dissociated Li^+ in the system. This makes the electrolyte softer and more susceptible to side reactions and aging effects, which increases the resistance of the cell and thus leads to a reduction in the specific capacity achieved.

4. Conclusions

In this work, a pre-mixed batch of PEO and LiTFSI powders with a molar ratio of 20:1 (EO:Li) is successfully extruded at a process temperature of 90 °C to produce solvent-free PEO:LiTFSI electrolytes. To investigate the effect of extruder setup on product quality, different screw designs with conveying, kneading and mixing elements were tested. In addition, the screw speed was varied from 5 to 15 rpm. The monitored process parameters, torque and pressure at the extruder die, are used to investigate the process stability and the influence of screw designs and applied screw speed on the process itself. Both parameters show a dependence on the screw design and the applied torque. While the torque increases with increasing screw speed and shows the smallest error at 5 rpm, the pressure at the extruder die shows no significant change with the applied screw speed. The most stable process, characterized by the smallest error bar of the monitored pressure, is achieved with screw design B. Microscopic observation shows that screw design B achieves the best mixing of PEO and LiTFSI, especially at high screw speeds. The determination of M_w also shows that screw design B gives the best result at high screw speeds. Here, we see the least loss of M_w indicating that this screw design best maintains the polymer properties during extrusion. DMA measurements show the influence of LiTFSI on the thermo-mechanical properties of PEO by shifting the T_m to a lower temperature and by reducing the overall mechanical strength. All produced PEO:LiTFSI electrolytes exhibit an ionic conductivity of $(1.1\text{--}1.8) \times 10^{-4} \text{ S cm}^{-1}$ at 80 °C, which is comparable with the literature indicating successful extrusion of PEO-based solid electrolytes. In addition, the M_w of all produced electrolytes is still high enough that the σ_{ionic} is not affected by the extrusion process itself. Even though the cycling test shows the highest loss in specific capacity of 15% over 20 cycles for screw design B, the comparison of the screw designs shows that screw design B, which contains kneading elements, is the most promising candidate for upscaling dry SPE production by extrusion. Nonetheless, the mechanical strength of the electrolytes produced should be reinforced to result in better cycling stability. This was not part of this work and will be addressed in future work.

Author Contributions: Conceptualization, K.P.; methodology, K.P.; validation, K.P.; formal analysis, K.P.; investigation, K.P.; writing—original draft preparation, K.P.; writing—review and editing, F.L. and J.S. All authors have read and agreed to the published version of the manuscript.

Funding: This research was funded by the Lower Saxony Ministry of Science and Culture within the framework of “Niedersächsisches Vorab” (grant no. ZN3402) and the Federal Ministry of Education and Research (BMBF).

Data Availability Statement: The data presented in this study are available within this article.

Acknowledgments: This research was conducted within the framework of the Fraunhofer project Center for Electrical Energy Storage and Systems ZESS.

Conflicts of Interest: The authors declare no conflicts of interest.

Appendix A

Table A1. σ_{ionic} of PEO:LiTFSI electrolytes prepared by solvent-based and solvent-free processing methods extracted from the literature.

Processing Method	Mw of PEO [g mol ⁻¹]	EO:Li	wLiTFSI [%]	Ionic Conductivity [Scm ⁻¹]	Source
solvent-based	5×10^6	6:1	0.52	1.00×10^{-4}	[55]
solvent-based	90 wt% 1×10^5 + 10 wt% 5×10^6	10:1	0.39	2.00×10^{-4}	[54]
solvent-based	1×10^5	10:1	0.39	7.00×10^{-4}	[56]
solvent-based	90 wt% 1×10^5 + 10 wt% 5×10^6	15:1	0.3	2.00×10^{-4}	[54]
solvent-based	90 wt% 1×10^5 + 10 wt% 5×10^6	20:1	0.25	2.00×10^{-4}	[54]
solvent-based	1×10^5	20:1	0.25	5.00×10^{-4}	[56]
solvent-based	90 wt% 1×10^5 + 10 wt% 5×10^6	25:1	0.21	1.50×10^{-4}	[54]
solvent-based	2×10^2	25:1	0.21	5.00×10^{-4}	[50]
solvent-based	1×10^3	25:1	0.21	1.00×10^{-3}	[50]
solvent-based	3.5×10^4	25:1	0.21	9.00×10^{-4}	[50]
solvent-based	90 wt% 1×10^5 + 10 wt% 5×10^6	30:1	0.18	1.00×10^{-4}	[54]
solvent-based	5×10^6	50:1	0.12	7.00×10^{-4}	[13]
solvent-based	5×10^6	50:1	0.12	8.00×10^{-4}	[55]
solvent-free	1×10^6 / 1×10^5	10:1	0.39	2.00×10^{-4}	[33]
solvent-free	-	10:1	0.39	5.00×10^{-4}	[53]
solvent-free	4×10^6	10:1	0.39	1.50×10^{-3}	[52]
solvent-free	4×10^6	15:1	0.3	2.00×10^{-3}	[51]

References

- Chen, Y.; Kang, Y.; Zhao, Y.; Wang, L.; Liu, J.; Li, Y.; Liang, Z.; He, X.; Li, X.; Tavajohi, N.; et al. A review of lithium-ion battery safety concerns: The issues, strategies, and testing standards. *J. Energy Chem.* **2021**, *59*, 83–99. [[CrossRef](#)]
- Wu, X.; Song, K.; Zhang, X.; Hu, N.; Li, L.; Li, W.; Zhang, L.; Zhang, H. Safety Issues in Lithium Ion Batteries: Materials and Cell Design. *Front. Energy Res.* **2019**, *7*, 65. [[CrossRef](#)]
- Larsson, F.; Andersson, P.; Blomqvist, P.; Mellander, B.-E. Toxic fluoride gas emissions from lithium-ion battery fires. *Sci. Rep.* **2017**, *7*, 10018. [[CrossRef](#)] [[PubMed](#)]
- Lebedeva, N.P.; Boon-Brett, L. Considerations on the Chemical Toxicity of Contemporary Li-Ion Battery Electrolytes and Their Components. *J. Electrochem. Soc.* **2016**, *163*, A821–A830. [[CrossRef](#)]
- Nedjalkov, A.; Meyer, J.; Köhring, M.; Doering, A.; Angelmahr, M.; Dahle, S.; Sander, A.; Fischer, A.; Schade, W. Toxic Gas Emissions from Damaged Lithium Ion Batteries—Analysis and Safety Enhancement Solution. *Batteries* **2016**, *2*, 5. [[CrossRef](#)]
- Peng, Y.; Yang, L.; Ju, X.; Liao, B.; Ye, K.; Li, L.; Cao, B.; Ni, Y. A comprehensive investigation on the thermal and toxic hazards of large format lithium-ion batteries with LiFePO₄ cathode. *J. Hazard. Mater.* **2020**, *381*, 120916. [[CrossRef](#)] [[PubMed](#)]
- Janek, J.; Zeier, W.G. A solid future for battery development. *Nat. Energy* **2016**, *1*, 16141. [[CrossRef](#)]
- Sun, C.; Liu, J.; Gong, Y.; Wilkinson, D.P.; Zhang, J. Recent advances in all-solid-state rechargeable lithium batteries. *Nano Energy* **2017**, *33*, 363–386. [[CrossRef](#)]
- Lau, J.; DeBlock, R.H.; Butts, D.M.; Ashby, D.S.; Choi, C.S.; Dunn, B.S. Sulfide Solid Electrolytes for Lithium Battery Applications. *Adv. Energy Mater.* **2018**, *8*, 1800933. [[CrossRef](#)]
- Ren, Y.; Chen, K.; Chen, R.; Liu, T.; Zhang, Y.; Nan, C.-W. Oxide Electrolytes for Lithium Batteries. *J. Am. Ceram. Soc.* **2015**, *98*, 3603–3623. [[CrossRef](#)]
- Mauger, A.; Armand, M.; Julien, C.M.; Zaghib, K. Challenges and issues facing lithium metal for solid-state rechargeable batteries. *J. Power Sources* **2017**, *353*, 333–342. [[CrossRef](#)]
- Wu, Y.; Wang, S.; Li, H.; Chen, L.; Wu, F. Progress in thermal stability of all-solid-state-Li-ion-batteries. *InfoMat* **2021**, *3*, 827–853. [[CrossRef](#)]
- Yue, L.; Ma, J.; Zhang, J.; Zhao, J.; Dong, S.; Liu, Z.; Cui, G.; Chen, L. All solid-state polymer electrolytes for high-performance lithium ion batteries. *Energy Storage Mater.* **2016**, *5*, 139–164. [[CrossRef](#)]

14. Placke, T.; Kloepsch, R.; Dühnen, S.; Winter, M. Lithium ion, lithium metal, and alternative rechargeable battery technologies: The odyssey for high energy density. *J. Solid. State Electrochem.* **2017**, *21*, 1939–1964. [[CrossRef](#)]
15. Ma, J.; Wang, Z.; Wu, J.; Gu, Z.; Xin, X.; Yao, X. In Situ Solidified Gel Polymer Electrolytes for Stable Solid–State Lithium Batteries at High Temperatures. *Batteries* **2023**, *9*, 28. [[CrossRef](#)]
16. Tong, B.; Song, Z.; Wu, H.; Wang, X.; Feng, W.; Zhou, Z.; Zhang, H. Ion transport and structural design of lithium-ion conductive solid polymer electrolytes: A perspective. *Mater. Futures* **2022**, *1*, 42103. [[CrossRef](#)]
17. Li, Z.; Liang, W.; Chen, J.; Song, L.; Xiong, T.; Xie, W.; Wu, S.; Hu, D.; Yao, X.; Peng, Z. In-depth Li⁺ transportation in three-dimensionalized nanodiamond network for improved liquid and solid lithium metal batteries. *Nano Energy* **2023**, *110*, 108370. [[CrossRef](#)]
18. Wang, Z.; Shen, L.; Deng, S.; Cui, P.; Yao, X. 10 μm-Thick High-Strength Solid Polymer Electrolytes with Excellent Interface Compatibility for Flexible All-Solid-State Lithium-Metal Batteries. *Adv. Mater.* **2021**, *33*, e2100353. [[CrossRef](#)] [[PubMed](#)]
19. Janek, J.; Zeier, W.G. Challenges in speeding up solid-state battery development. *Nat. Energy* **2023**, *8*, 230–240. [[CrossRef](#)]
20. Arya, A.; Sharma, A.L. Polymer electrolytes for lithium ion batteries: A critical study. *Ionics* **2017**, *23*, 497–540. [[CrossRef](#)]
21. Yang, J.; Wang, X.; Zhang, G.; Ma, A.; Chen, W.; Shao, L.; Shen, C.; Xie, K. High-Performance Solid Composite Polymer Electrolyte for all Solid-State Lithium Battery through Facile Microstructure Regulation. *Front. Chem.* **2019**, *7*, 388. [[CrossRef](#)] [[PubMed](#)]
22. Jinisha, B.; Anilkumar, K.M.; Manoj, M.; Pradeep, V.S.; Jayalekshmi, S. Development of a novel type of solid polymer electrolyte for solid state lithium battery applications based on lithium enriched poly (ethylene oxide) (PEO)/poly (vinyl pyrrolidone) (PVP) blend polymer. *Electrochim. Acta* **2017**, *235*, 210–222. [[CrossRef](#)]
23. Chen, F.; Yang, D.; Zha, W.; Zhu, B.; Zhang, Y.; Li, J.; Gu, Y.; Shen, Q.; Zhang, L.; Sadoway, D.R. Solid polymer electrolytes incorporating cubic Li₇La₃Zr₂O₁₂ for all-solid-state lithium rechargeable batteries. *Electrochim. Acta* **2017**, *258*, 1106–1114. [[CrossRef](#)]
24. Kimura, K.; Yajima, M.; Tominaga, Y. A highly-concentrated Poly(ethylene carbonate)-based electrolyte for all-solid-state Li battery working at room temperature. *Electrochim. Commun.* **2016**, *66*, 46–48. [[CrossRef](#)]
25. Polu, A.R.; Rhee, H.-W.; Kim, D.K. New solid polymer electrolytes (PEO20–LiTDI–SN) for lithium batteries: Structural, thermal and ionic conductivity studies. *J. Mater. Sci. Mater. Electron.* **2015**, *26*, 8548–8554. [[CrossRef](#)]
26. Zhang, X.; Wang, S.; Xue, C.; Xin, C.; Lin, Y.; Shen, Y.; Li, L.; Nan, C.-W. Self-Suppression of Lithium Dendrite in All-Solid-State Lithium Metal Batteries with Poly(vinylidene difluoride)-Based Solid Electrolytes. *Adv. Mater.* **2019**, *31*, e1806082. [[CrossRef](#)]
27. Miao, R.; Liu, B.; Zhu, Z.; Liu, Y.; Li, J.; Wang, X.; Li, Q. PVDF-HFP-based porous polymer electrolyte membranes for lithium-ion batteries. *J. Power Sources* **2008**, *184*, 420–426. [[CrossRef](#)]
28. Foran, G.; Mankovsky, D.; Verdier, N.; Lepage, D.; Prébé, A.; Aymé-Perrot, D.; Dollé, M. The Impact of Absorbed Solvent on the Performance of Solid Polymer Electrolytes for Use in Solid-State Lithium Batteries. *iScience* **2020**, *23*, 101597. [[CrossRef](#)]
29. Liu, Y.; Zhang, R.; Wang, J.; Wang, Y. Current and future lithium-ion battery manufacturing. *iScience* **2021**, *24*, 102332. [[CrossRef](#)] [[PubMed](#)]
30. Schünemann, J.-H.; Dreger, H.; Bockholt, H.; Kwade, A. Smart Electrode Processing for Battery Cost Reduction. *ECS Trans.* **2016**, *73*, 153–159. [[CrossRef](#)]
31. Schnell, J.; Günther, T.; Knoche, T.; Vieider, C.; Köhler, L.; Just, A.; Keller, M.; Passerini, S.; Reinhart, G. All-solid-state lithium-ion and lithium metal batteries—Paving the way to large-scale production. *J. Power Sources* **2018**, *382*, 160–175. [[CrossRef](#)]
32. Appetecchi, G.B.; Hassoun, J.; Scrosati, B.; Croce, F.; Cassel, F.; Salomon, M. Hot-pressed, solvent-free, nanocomposite, PEO-based electrolyte membranes. *J. Power Sources* **2003**, *124*, 246–253. [[CrossRef](#)]
33. Gray, F.M.; MacCallum, J.R.; Vincent, C.A. Poly(ethylene oxide)—LiCF₃SO₃—polystyrene electrolyte systems. *Solid. State Ion.* **1986**, *18*, 282–286. [[CrossRef](#)]
34. Wang, L.; Li, X.; Yang, W. Enhancement of electrochemical properties of hot-pressed Poly(ethylene oxide)-based nanocomposite polymer electrolyte films for all-solid-state lithium polymer batteries. *Electrochim. Acta* **2010**, *55*, 1895–1899. [[CrossRef](#)]
35. Mejía, A.; Devaraj, S.; Guzmán, J.; Del Lopez Amo, J.M.; García, N.; Rojo, T.; Armand, M.; Tiemblo, P. Scalable plasticized polymer electrolytes reinforced with surface-modified sepiolite fillers—A feasibility study in lithium metal polymer batteries. *J. Power Sources* **2016**, *306*, 772–778. [[CrossRef](#)]
36. Helmers, L.; Froböse, L.; Friedrich, K.; Steffens, M.; Kern, D.; Michalowski, P.; Kwade, A. Sustainable Solvent-Free Production and Resulting Performance of Polymer Electrolyte-Based All-Solid-State Battery Electrodes. *Energy Technol.* **2021**, *9*, 2000923. [[CrossRef](#)]
37. Froboese, L.; Groffmann, L.; Monsees, F.; Helmers, L.; Loellhoeffel, T.; Kwade, A. Enhancing the Lithium Ion Conductivity of an All Solid-State Electrolyte via Dry and Solvent-Free Scalable Series Production Processes. *J. Electrochem. Soc.* **2020**, *167*, 20558. [[CrossRef](#)]
38. Edman, L.; Ferry, A.; Doeffer, M.M. Slow recrystallization in the polymer electrolyte system Poly(ethylene oxide)n–LiN(CF₃SO₂)₂. *J. Mater. Res.* **2000**, *15*, 1950–1954. [[CrossRef](#)]
39. Marzantowicz, M.; Dygas, J.R.; Krok, F.; Nowiński, J.L.; Tomaszewska, A.; Florjańczyk, Z.; Zygałdo-Monikowska, E. Crystalline phases, morphology and conductivity of PEO:LiTFSI electrolytes in the eutectic region. *J. Power Sources* **2006**, *159*, 420–430. [[CrossRef](#)]
40. Zhang, H.; Liu, C.; Zheng, L.; Xu, F.; Feng, W.; Li, H.; Huang, X.; Armand, M.; Nie, J.; Zhou, Z. Lithium bis(fluorosulfonyl)imide/poly(ethylene oxide) polymer electrolyte. *Electrochim. Acta* **2014**, *133*, 529–538. [[CrossRef](#)]

41. Nair, J.R.; Imholt, L.; Brunklaus, G.; Winter, M. Lithium Metal Polymer Electrolyte Batteries: Opportunities and Challenges. *Electrochem. Soc. Interface* **2019**, *28*, 55–61. [[CrossRef](#)]
42. Crowley, M.M. Physicochemical and Mechanical Characterization of Hot-Melt Extruded Dosage Forms. Ph.D. Thesis, The University of Texas at Austin ProQuest Dissertation & Theses, Austin, TX, USA, 2003.
43. Crowley, M.M.; Zhang, F.; Koleng, J.J.; McGinity, J.W. Stability of polyethylene oxide in matrix tablets prepared by hot-melt extrusion. *Biomaterials* **2002**, *23*, 4241–4248. [[CrossRef](#)] [[PubMed](#)]
44. Fenton, D.E.; Parker, J.M.; Wright, P.V. Complexes of alkali metal ions with Poly(ethylene oxide). *Polymer* **1973**, *14*, 589. [[CrossRef](#)]
45. Platen, K.; Langer, F.; Bayer, R.; Hollmann, R.; Schwenzel, J.; Busse, M. Influence of Molecular Weight and Lithium Bis(trifluoromethanesulfonyl)imide on the Thermal Processability of Poly(ethylene oxide) for Solid-State Electrolytes. *Polymers* **2023**, *15*, 3375. [[CrossRef](#)] [[PubMed](#)]
46. Borghini, M.C.; Mastragostino, M.; Passerini, S.; Scrosati, B. Electrochemical Properties of Polyethylene Oxide—Li [(CF₃SO₂)₂N]—Gamma—LiAlO₂ Composite Polymer Electrolytes. *J. Electrochem. Soc.* **1995**, *142*, 2118–2121. [[CrossRef](#)]
47. Mindemark, J.; Lacey, M.J.; Bowden, T.; Brandell, D. Beyond PEO—Alternative host materials for Li + -conducting solid polymer electrolytes. *Prog. Polym. Sci.* **2018**, *81*, 114–143. [[CrossRef](#)]
48. Kohlgrüber, K. (Ed.) *Co-Rotating Twin-Screw Extruders: Applications*; Hanser Publications: Munich, Germany; Cincinnati, OH, USA, 2021; ISBN 978-1-56990-781-8.
49. Marzantowicz, M.; Dygas, J.R.; Krok, F.; Florjańczyk, Z.; Zygałdo-Monikowska, E. Influence of crystallization on dielectric properties of PEO:LiTFSI polymer electrolyte. *J. Non-Cryst. Solids* **2006**, *352*, 5216–5223. [[CrossRef](#)]
50. Devaux, D.; Bouchet, R.; Glé, D.; Denoyel, R. Mechanism of ion transport in PEO/LiTFSI complexes: Effect of temperature, molecular weight and end groups. *Solid. State Ion.* **2012**, *227*, 119–127. [[CrossRef](#)]
51. Kim, Y.-T.; Smotkin, E.S. The effect of plasticizers on transport and electrochemical properties of PEO-based electrolytes for lithium rechargeable batteries. *Solid. State Ion.* **2002**, *149*, 29–37. [[CrossRef](#)]
52. Kim, G.T.; Appeteccchi, G.B.; Carewska, M.; Joost, M.; Balducci, A.; Winter, M.; Passerini, S. UV cross-linked, lithium-conducting ternary polymer electrolytes containing ionic liquids. *J. Power Sources* **2010**, *195*, 6130–6137. [[CrossRef](#)]
53. Graebe, H.; Netz, A.; Baesch, S.; Haerdtnner, V.; Kwade, A. A Solvent-Free Electrode Coating Technique for All Solid State Lithium Ion Batteries. *ECS Trans.* **2017**, *77*, 393–401. [[CrossRef](#)]
54. Maurel, A.; Armand, M.; Grugeon, S.; Fleutot, B.; Davoisne, C.; Tortajada, H.; Courty, M.; Panier, S.; Dupont, L. Poly(ethylene oxide)—LiTFSI Solid Polymer Electrolyte Filaments for Fused Deposition Modeling Three-Dimensional Printing. *J. Electrochem. Soc.* **2020**, *167*, 70536. [[CrossRef](#)]
55. Marzantowicz, M.; Dygas, J.R.; Krok, F.; Łasińska, A.; Florjańczyk, Z.; Zygałdo-Monikowska, E.; Affek, A. Crystallization and melting of PEO:LiTFSI polymer electrolytes investigated simultaneously by impedance spectroscopy and polarizing microscopy. *Electrochim. Acta* **2005**, *50*, 3969–3977. [[CrossRef](#)]
56. Abels, G. Grenzschichtverhalten von Polymerelektrolyten gegenüber Elektrodenmaterialien für Zukünftige Hochenergie-Lithium-Ionen Sekundärbatterien. Doctoral Dissertation, Universität Bremen, Bremen, Germany, 2022.
57. Hallinan, D.T.; Balsara, N.P. Polymer Electrolytes. *Annu. Rev. Mater. Res.* **2013**, *43*, 503–525. [[CrossRef](#)]

Disclaimer/Publisher's Note: The statements, opinions and data contained in all publications are solely those of the individual author(s) and contributor(s) and not of MDPI and/or the editor(s). MDPI and/or the editor(s) disclaim responsibility for any injury to people or property resulting from any ideas, methods, instructions or products referred to in the content.